Research Article

Ping Zhang, Cheng Li, and Jian Mao*

A multiscale and dual-loss network for pulmonary nodule classification

https://doi.org/10.1515/comp-2025-0030 received September 27, 2024; accepted April 28, 2025

Abstract: Detecting malignancy in pulmonary nodules holds significant clinical importance, yet existing image classification methods often struggle with inadequate feature integration and ineffective loss functions. This study proposes two innovative strategies to address these limitations: first, we introduce a multiscale feature weighted fusion technique that enhances the integration of features across different scales, allowing the model to prioritize critical pixel locations essential for accurate diagnosis. Second, we combine contrastive loss with binary cross-entropy within our training framework to improve learning from both similarities and differences among paired samples, which fosters better discrimination between similar nodules while maintaining sensitivity to variations across classes. Besides, our proposed methodologies demonstrate promising performance improvements in detecting pulmonary nodule malignancy, leading to enhanced performance and reliability compared to conventional approaches.

Keywords: pulmonary nodules, image classification, multiscale feature fusion, contrastive loss

1 Introduction

Lung cancer, with its high incidence and mortality rates, necessitates early diagnosis to improve survival outcomes. The classification of pulmonary nodules (as shown in Figure 1) as benign or malignant is essential for identifying

potential malignancies and guiding treatment plans [1,2].

Cheng Li: Qingdao University of Science and Technology, Qingdao, 266061, P. R. China, e-mail: 1chcheng1@163.com

Traditionally, physicians evaluate these nodules using computed tomography (CT) images; however, this process can be time consuming and relies heavily on individual experience, which may affect both efficiency and accuracy. To address these challenges, computer-aided diagnosis (CAD) systems [3,4] have emerged as valuable tools that utilize advanced image processing and machine learning algorithms to automatically analyze CT images. By learning from extensive datasets to detect subtle imaging features, CAD systems leverage artificial intelligence to aid physicians in making faster and more accurate decisions, thereby significantly advancing the assessment of pulmonary nodules and enhancing modern medical imaging. Previously, many studies have indicated that machine learning methodologies play a crucial role in advancing the diagnostic accuracy of pulmonary nodules. For instance, Liu et al. developed a systematic approach that quantifies radiological traits and emphasizes semantic imaging features for predicting malignancy, resulting in enhanced predictive accuracy [5]. In another study, Ferreira et al.'s random forest algorithm demonstrated superior performance compared to other classifiers; notably, a decision tree using only two features achieved comparable sensitivity and specificity [6]. Meanwhile, Tu et al. effectively combined localized thin-section CT with radiomics feature extraction and machine learning to accurately classify early-detected pulmonary nodules, thereby reducing false positives while improving malignancy differentiation [7]. Yang et al. highlighted essential nodular features through a review focused on ground-glass opacity nodules, which were vital for developing effective prediction models [8]. Uthoff et al. contributed by standardizing perinodular features, while Yamada et al. improved classification accuracy with positron emission tomographic/CT images [9,10]. Furthermore, Chen et al.'s method had outperformed existing approaches in malignancy prediction; similarly, Liu et al.'s integration of CT findings with CEA levels yielded superior predictions [11,12]. Recently, many investigations have highlighted the effectiveness of deep learning techniques, particularly convolutional neural networks (CNNs), in detecting and classifying pulmonary nodules from CT scans. Wang et al.

^{*} Corresponding author: Jian Mao, Qingdao Central Hospital, University of Health and Rehabilitation Sciences, Qingdao, 266042, P. R. China, e-mail: Javamars_qd@outlook.com Ping Zhang: Qingdao Central Hospital, University of Health and Rehabilitation Sciences, Qingdao, 266042, P. R. China, e-mail: zhangpingQDCN@outlook.com

2 — Ping Zhang et al. DE GRUYTER

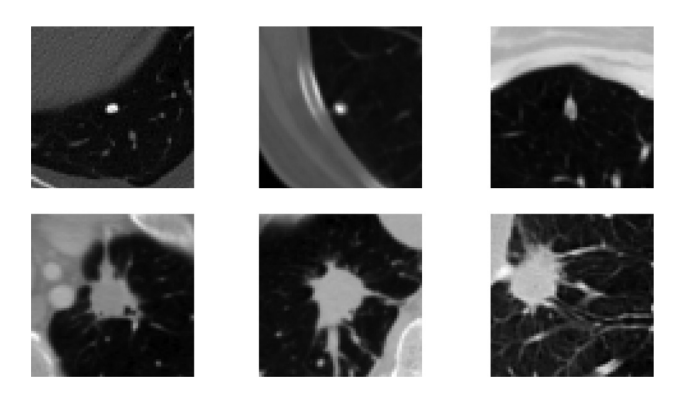


Figure 1: The samples of different pulmonary nodules.

introduced a hybrid CNN model that enhanced malignancy risk assessment accuracy by integrating global and local features, surpassing traditional texture and shape-based methods [13]. Dou et al. developed a three-dimensional CNN that significantly reduced false positives by incorporating multilevel information, thereby improving detection efficiency [14]. Jin et al.'s deep 3D residual CNN further advanced lung cancer diagnosis by effectively targeting false positives [15]. Additionally, Feng et al. created a weaklysupervised CNN for automated nodule segmentation using image-level labels, successfully localizing nodules in CT images [16]. The integration of transfer learning has also played a crucial role; Zhao et al.'s approach outperformed other CNN strategies in distinguishing malignant from benign nodules [17]. Recent innovations such as the multiscale gradual integration CNN had shown significant improvements on datasets like LUNA16 [18]. Moreover, the growing body of literature indicated that hybrid models, attention mechanisms, and ensemble learning strategies – such as those developed by Yuans et al. and Xu et al. – were essential for achieving high sensitivity and accuracy in lung cancer risk assessment [19,20]. These advancements underscore the continuous evolution of deep learning methodologies within medical imaging, highlighting their potential to transform clinical practices and improve patient outcomes in lung cancer detection and management.

Previous methods in image classification for detecting pulmonary nodule malignancy have made significant strides, but they still face limitations that impact their effectiveness. A major issue is the inadequate integration of features from various scales, which leads to a lack of focus on the discriminative traits necessary for accurate diagnosis. Traditional approaches often rely on single-scale feature extraction and can overlook critical contextual information, affecting performance when distinguishing between benign and malignant nodules. In addition,

conventional loss functions like binary cross-entropy (BCE) do not fully leverage the relationships among paired samples, impairing generalization across classes. To address these challenges, we propose two innovative strategies: first, we implement multiscale feature weighted fusion (MFWF) to enhance information integration across different scales through spatial resizing and the computation of a weight matrix that emphasizes crucial pixel positions. This pixel-wise weight matrix guides the weighted fusion of multiscale features, prioritizing the most salient information. By effectively combining hierarchical details with semantic information, this approach enhances the model's ability to capture complex patterns and improves its discriminability. Second, the contrastive loss excels at pulling similar pairs closer together in the embedding space and pushing dissimilar pairs farther apart, effectively emphasizing relative relationships. Simultaneously, the BCE loss ensures the model remains sensitive to variations across differing classes by providing a consistent supervisory signal focused on classification accuracy for each sample individually. Therefore, to leverage these strengths, we combine contrastive loss with BCE loss in a dual-loss training framework. This approach not only enhances discrimination among similar samples by finetuning the embedding space for closely related examples, but also maintains robust sensitivity to interclass variance, preventing the model from collapsing distinguishable categories into indistinguishable clusters. Overall, these integrated methodologies improve classification performance and bolster the model's ability to generalize across diverse patient datasets encountered in clinical settings. The main contributions of this article can be summarized as follows:

- We introduce the MFWF that enhances the integration of features across different scales, allowing the model to focus on critical pixel positions and improving its sensitivity to discriminative characteristics essential for accurate diagnosis.
- By employing dual loss, we enable the model to better learn from similarities and differences among paired samples, which enhances discrimination among similar nodules while maintaining sensitivity to class variations.
- Our proposed methods exhibit promising performance in detecting pulmonary nodule malignancy, highlighting improvements in accuracy and reliability when compared to existing approaches.

The rest of this article is organized as follows: In Section 2, it outlines our proposed MFWF approach and the dual-loss training strategy, detailing the technical implementation and theoretical foundations underpinning these methods. Subsequently, in Section 3, we present the

experimental setup, including the datasets utilized for evaluation and the metrics employed to assess performance. Finally, we conclude with a summary of key findings and future directions for research in this domain in Section 4.

nodules, we propose the MFWF module. Furthermore, to enhance discrimination among paired samples while preserving sensitivity to class variations, we have designed a dualloss strategy that complements this approach.

2 Methodology

The main structure of this article is illustrated in Figure 2, featuring a primary architecture based on the ResNet network. To effectively extract multiscale features of pulmonary

2.1 Revisit of residual block

In this section, we first revisit the residual block, which serves as the fundamental building block of our architectures. The key innovation that the residual block

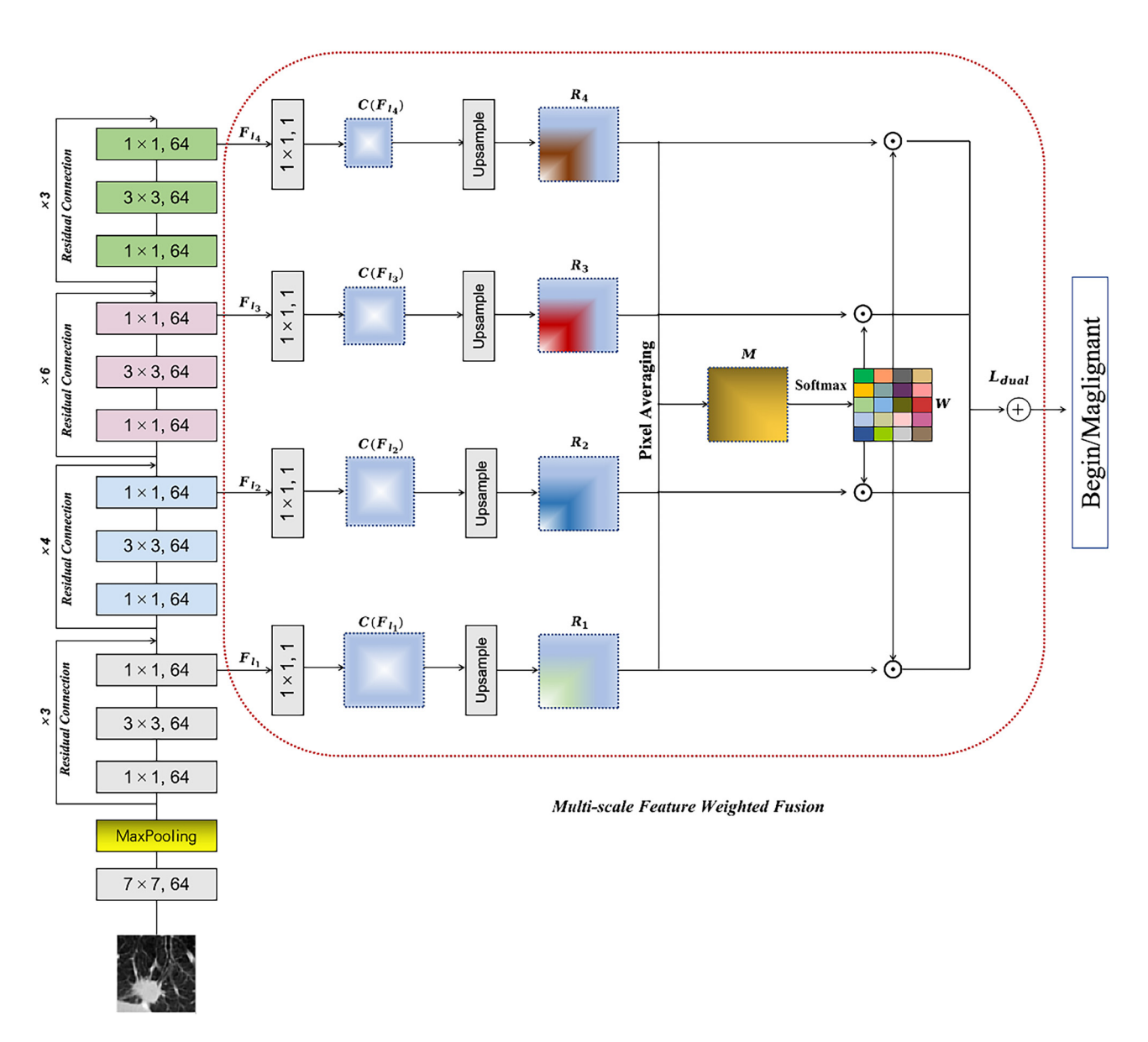


Figure 2: The proposed model is structured based on the ResNet architecture. A multiscale feature fusion module is introduced to effectively extract multiscale features from pulmonary nodules. Furthermore, a dual-loss strategy is designed to enhance discrimination among paired samples while preserving sensitivity to class variations, complementing this approach.

introduces is the concept of skip connections, which facilitate gradient flow through the network and mitigate issues related to vanishing gradients. The mathematical formulation of a basic residual block can be expressed as follows:

$$\mathbf{v} = \mathcal{F}(\mathbf{x}, \{\theta\}) + \mathbf{x},\tag{1}$$

where \mathbf{x} represents the input to the residual block, $\mathcal{F}(\mathbf{x}, \{\theta\})$ denotes a series of operations parameterized by weights $\{\theta\}$, and \mathbf{y} is the output of the residual block. The addition operation in equation (1) allows for the identity mapping from input \mathbf{x} , enabling a direct path for gradients during backpropagation. To elaborate further, each residual block typically consists of two or more convolutional layers along with batch normalization and ReLU activation. The common configuration within a residual block could be given as follows:

$$\mathbf{y} = \mathcal{F}(\mathcal{F}(\mathbf{x}, \theta_1), \theta_2) + \mathbf{x}. \tag{2}$$

This structure provides not only depth but also enhances representational capacity while ensuring that valuable features are retained throughout multiple layers.

2.2 Multiscale feature weighted fusion

The process begins with inputting an image $I \in \mathbb{R}^{H \times W \times C}$, where H represents the height, W denotes the width, and C is the number of channels. By applying the ResNet network, this image undergoes multiple convolutional layers and activation functions to extract features at various scales and abstraction levels. At this stage, we obtain corresponding feature maps for ith layer, the output feature map from layer l_i can be expressed as follows:

$$F_{l_i} = f_{l_i}(I) \in \mathbb{R}^{H_{l_i} \times W_{l_i} \times D_{l_i}}.$$
(3)

To reduce dimensionality while enhancing the expressive power of features, we apply a 1×1 convolutional layer to each extracted feature map. This not only allows us to reduce the channel dimensions while preserving spatial information but also enhances the model's ability to capture nonlinear representations. This operation can be described by the following equation:

$$C(F_{l_i}) = W^{(i)*}F_{l_i} + b^{(i)},$$
 (4)

where $W^{(i)}$ represents the weights and $b^{(i)}$ is its corresponding bias term. Next, for all processed multiscale feature maps, we perform spatial resizing to unify their dimensions to a specified size H_f , W_f . This step is essential for effective combination and fusion of different scales

without losing important information or details. The adjustment can be formulated as follows:

$$R_i = R(C(F_{l_i}), H_f, W_f).$$
 (5)

After resizing, we obtain a set of new feature maps expressed as follows:

$$R_{\text{features}} = \{R_1, R_2, ..., R_n\}.$$
 (6)

Subsequently, at each pixel position (h, w), we calculate the average value across different scales to construct a weight that provides insight into which scale contributes more significantly. This operation can be defined as follows:

$$M(h, w) = \frac{1}{n} \sum_{i=1}^{n} R_i(h, w).$$
 (7)

Following this calculation, we build a weight matrix reflecting the importance of each scale through normalization:

$$W(h, w) = \frac{M(h, w)}{\sum_{i=1}^{n} M_i(h, w)}.$$
 (8)

Once these steps are completed, we acquire a weight matrix for every pixel that emphasizes important features. Next, these weighted feature maps are summation combined to derive a final fused representation defined by the following equation:

$$F_{\text{final}} = \left(\sum_{t=1}^{n} W_t \odot R_t\right). \tag{9}$$

Finally, to achieve classification objectives, we employ a linear layer yielding class predictions according to:

$$P(y|I) = g(F_{\text{final}}, W_p, b_p), \tag{10}$$

where $g(\cdot)$ refers to softmax, and parameters W_p , b_p , represent weights and biases learned by the classifier.

2.3 Dual-loss strategy

In the binary classification task of pulmonary nodule malignancy, we first prepare a dataset consisting of pairs of pulmonary nodule images along with their corresponding labels. For each input image pair (I_1 , I_2), where I_1 and I_2 represent two pulmonary nodule images, if both belong to the same category (either both benign or both malignant), then the label is set to y = 0; if they belong to different categories (one benign and the other malignant), then the label is set to y = 1. Next, we use the proposed

ResNet as a feature extractor by loading pre-trained weights and removing the last fully connected layer, retaining only the part used for generating feature embeddings. During this process, for each input image I_s , we obtain the feature representation through forward propagation:

$$Z_{\rm S} = f(I_{\rm S}),\tag{11}$$

where Z_s is the output feature vector, and f denotes the feedforward process through ResNet. Subsequently, to optimize model performance, we first define Euclidean distance to measure the difference in feature embeddings between the two pulmonary nodule images:

$$D(Z_1, Z_2) = ||Z_1 - Z_2||. (12)$$

Then we compute the overall contrastive loss $L_{\text{contrastive}}(y, D(Z_1, Z_2))$:

$$L_c(y, D(Z_1, Z_2)) = \begin{cases} 0.5D(Z_1, Z_2)^2 & \text{if } y = 0 \\ 0.5(\max(0, m - D(Z_1, Z_2)))^2 & \text{if } y = 1. \end{cases}$$
 (13)

In this context, $L_c(y, D(Z_1, Z_2))$ is the contrastive loss; when samples are from the same class (i.e., y = 0), we minimize their distance, whereas when samples are from different classes (i.e., y = 1), we desire that their distance exceeds some threshold m. Simultaneously, we use BCE loss to assess how well the network predicts given inputs. Corresponding to each category, the network produces a logits value that is transformed into probability via a sigmoid function:

$$p(y|I_s) = \sigma(z_s), \quad z_s = g(I_s),$$
 (14)

where $p(y|I_s)$ indicates the probability of malignancy given provided pulmonary nodule image I_s and z_s is its logits value after mapping; while function $g(I_s)$ maps inputs into output space via the neural network structure. Thus, the BCE loss can be defined as follows:

$$L_{\text{bce}}(y, p(y|I)) = -[y \log(p(y|I)) + (1 - y) \log(1 - p(y|I))]. \quad (15)$$

Finally, these two losses are combined into an overall loss function:

$$L_{\text{dual}} = L_{\text{contrastive}} + L_{\text{bce}},$$
 (16)

where L_{dual} represents total loss including contrastive loss and binary cross-entropy loss. During training, paired data will be passed into model preferentially, followed by performing forward propagation in every epoch leading towards obtaining feature embedding accordingly. Full consideration regarding total loss would include comprehensive optimization schemes toward respective parameter updates throughout iterations.

3 Experiment

In this section, we outline a series of experiments aimed at validating the effectiveness of our proposed methodologies for detecting pulmonary nodule malignancy. We begin by describing the dataset utilized, along with the implementation details and evaluation metrics. Following this, we conduct a systematic set of experiments to assess and confirm the efficacy of our proposed model.

3.1 Datasets

The LIDC-IDRI (Lung Image Database Consortium and Image Database Resource Initiative, https://www. cancerimagingarchive.net/collection/lidc-idri/) is a public database dedicated to the detection and classification of pulmonary nodules. It consists of CT scan images from 1,018 patients, with slice thicknesses varying from 0.6 to 5 mm. To ensure accuracy, each nodule's diagnostic information including location, diameter, malignancy classified on a scale of 1 to 5, calcification level, and spiculation - has been independently annotated by four radiologists. This research aims to develop a network that classifies nodules as benign or malignant based on a voting strategy; specifically, if at least half of the experts rate a nodule above 3, it will be classified as malignant; otherwise, it will be deemed benign. To simplify model complexity, only the center cross-section image of each nodule is used as input.

3.2 Implementation details

The classification network was developed in an experimental environment using Keras, leveraging the power of an Nvidia GTX 3090 GPU. In addition, we implemented a learning rate adaptation strategy known as ReduceLROnPlateau, which adjusts the learning rate based on validation performance metrics. To further enhance model generalization, we applied various data augmentation techniques such as random rotations, vertical and horizontal flips, and brightness adjustments. The experimental results are validated by cross-validation to ensure generalizability, where performance metrics are averaged over all folds.

6 — Ping Zhang et al. DE GRUYTER

3.3 Evaluation metrics

Accuracy measures the overall model performance in correctly classifying instances. It is calculated as the ratio of true positives (TP), which are correctly identified positive cases, and true negatives (TN), which are correctly identified negative cases, to the total number of instances assessed (including false positives (FP) and false negatives (FN)):

Accuracy =
$$\frac{TP + TN}{TP + TN + FP + FN}.$$
 (17)

Sensitivity indicates the model's ability to identify actual positive instances. It is defined as the proportion of true positives relative to all actual positives (TP plus FN):

Sensitivity =
$$\frac{TP}{TP + FN}$$
. (18)

Specificity assesses the model's effectiveness in identifying negative instances. It expresses the proportion of TN out of all actual negatives (TN plus FP):

Specificity =
$$\frac{TN}{TN + FP}$$
. (19)

The area under receiver operating characteristic (ROC) curve (AUC) summarizes the model's capability to discriminate between classes; higher values indicate better performance. AUC is evaluated by plotting the true positive rate against the false positive rate across various thresholds.

3.4 Evaluation of multiscale feature weighted fusion

This experiment evaluates the impact of MFWF on model performance. A comparison is made between the classification different evaluation metrics of the model employing the proposed MFWF and that without (w/o) MFWF as shown in Table 1. The results indicate an effective enhancement in the recognition of critical features across varying scales, suggesting that the integration of information from multiple scales allows for improved attention to essential characteristics relevant to accurate classification. This

Table 1: Evaluation of multiscale feature weighted fusion

	Accuracy (%)	Sensitivity (%)	Specificity (%)	AUC
w/ o MFWF	90.12	90.00	90.23	0.902
w/ MFWF	91.34	92.44	90.26	0.924

improvement highlights the effectiveness of our approach in addressing the limitations associated with single-scale methods, ultimately leading to better diagnostic capabilities in classifying pulmonary nodules.

3.5 Different fusion modes of MFWF

In the MFWF process, we examine various fusion techniques such as averaging, concatenation, and linear fusion alongside simple summation for integrating features from different layers. As shown in Figure 3, our experimental results demonstrate that summation consistently outperforms the other methods due to its ability to emphasize significant features captured in deeper layers while avoiding dimensionality issues present in concatenation. Unlike averaging, which dilutes key information by giving equal weight to all inputs, summation effectively enhances classification performance by retaining critical details. While linear blending shows promise in specific contexts through its adaptability, it does not achieve the robust performance exhibited by the summation method.

3.6 Impact of dual-loss training strategy

The experiments conducted to evaluate the benefits of combining $L_{\rm dual}$ with $L_{\rm contrastive}$ and $L_{\rm bce}$ demonstrate enhanced generalization performance, as shown in Table 2. The dual-loss strategy ultimately achieves superior results. This improvement can be attributed to its ability to facilitate learning from both similarities and differences among paired samples. By integrating both types of information, the model gains a more nuanced understanding of the relationships between benign and malignant nodules, surpassing the performance of using a single loss function ($L_{\rm bce}$ or $L_{\rm contrastive}$) alone.

3.7 The integration of various input sizes

In the experiment, image sizes of 64×64 , 96×96 , 128×128 , 256×256 , and 512×512 are utilized. As illustrated in Figure 4, the results show that the model performs best at an input size of 128×128 . This optimal performance stems from the ability to balance sufficient detail capture with manageable computational complexity. At this size, the model effectively retains important features

DE GRUYTER

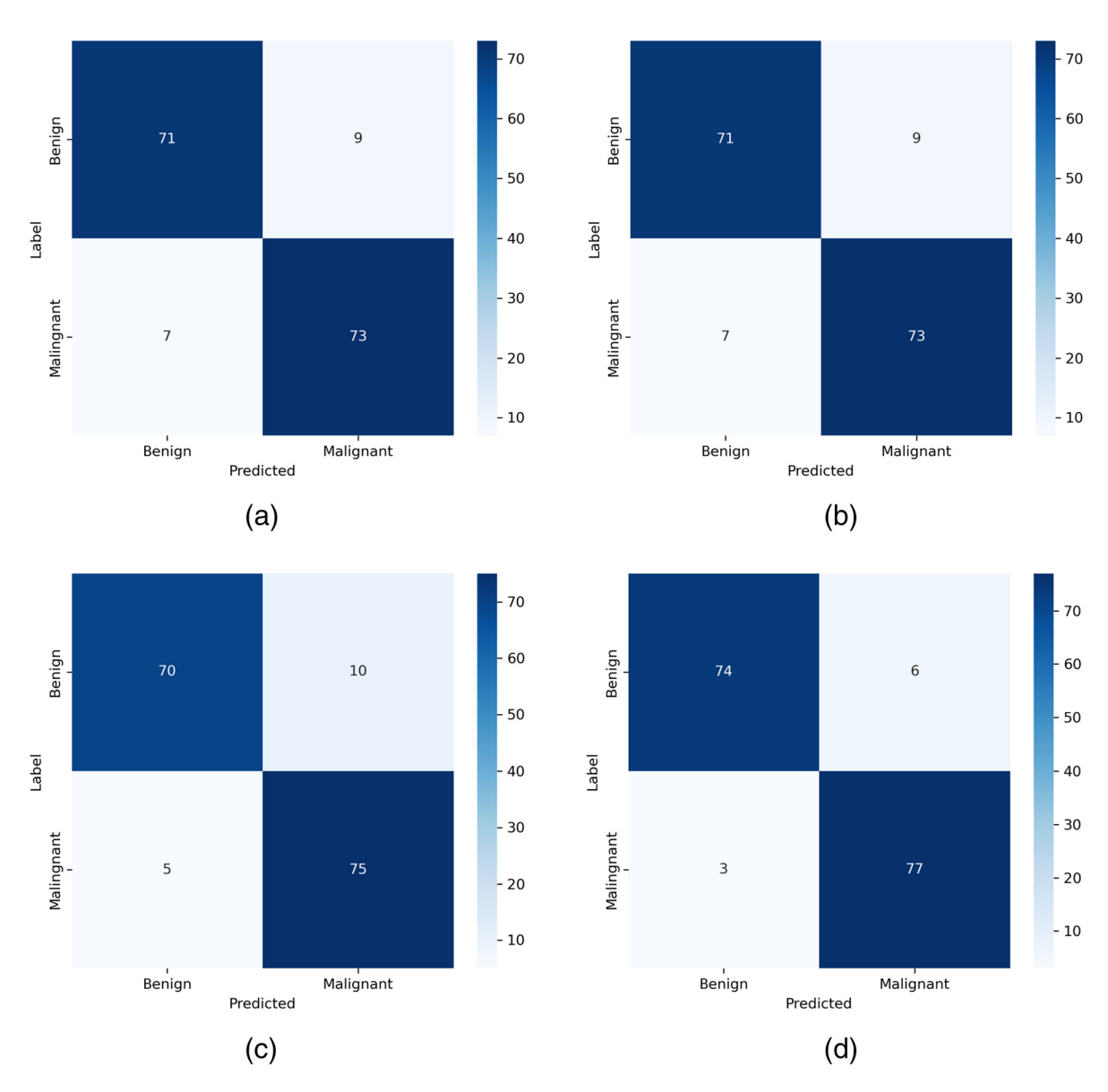


Figure 3: Different fusion modes of MFWF. a, b, c, d represents the averaging, concatenation, linear, and summation, respectively.

necessary for classification while avoiding information loss seen in smaller sizes and excessive noise found in larger sizes. Ultimately, the choice of 128 × 128 enables efficient focus on significant patterns, leading to improved feature extraction and enhanced classification accuracy in deep learning models.

3.8 Comparison with state-of-the-art models

To validate the proposed methods further, a comparative analysis is implemented against several state-of-the-art image classification models currently employed for malignancy detection in pulmonary nodules. Notably, since the

Table 2: Impact of dual-loss training strategy

	Accuracy (%)	Sensitivity (%)	Specificity (%)	AUC
$L_{ m bce}$	90.72	91.53	90.01	0.905
$L_{ m contrastive}$	89.16	90.02	88.37	0.868
$L_{\rm bce}$ + $L_{\rm contrastive}$	91.34	92.44	90.26	0.924

8 — Ping Zhang et al. DE GRUYTER

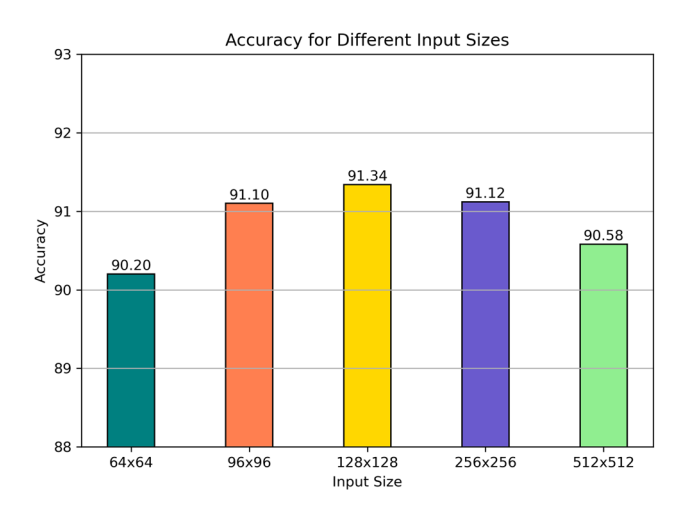


Figure 4: The integration of various input sizes.

sizes of each method in the original research is not the same, for a fair comparison, we reemploy those methods on the same data to validate the effectiveness of our proposed method. All the hyperparameters are obeyed the original settings. Here, we compare those methods as follow: Nibali et al. [21], Shen et al. [22], Zhang et al. [23], Wang et al. [24], Zhang et al. [25], Huo et al. [26], Ding et al. [27] (only using the single stream and modality), and Manzari et al. [28]. As shown in Table 3 and Figure 5, the results indicate that the proposed approach consistently outperforms existing methodologies across all evaluation metrics. Notably, we conduct paired t-tests to compare our proposed method with other existing approaches, and the p-values obtained from these comparisons are all below 0.05, thereby confirming the statistical significance of the reported improvements. Furthermore, this improved performance can be attributed to the effective integration of multiscale features employed during training, which enhances the model's ability to discern subtle differences between benign and malignant nodules. In addition, the use of contrastive loss facilitates better learning from

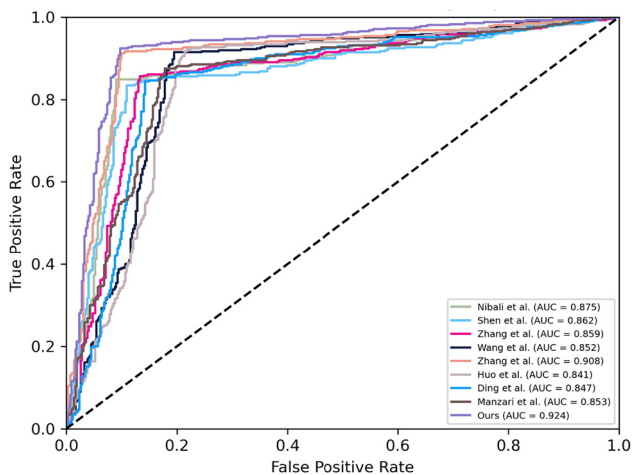


Figure 5: The ROC comparisons with state-of-the-art methods.

similar samples, contributing to an overall increase in diagnostic accuracy and reliability. These findings underscore the advancements achieved by our proposed methods in enhancing the classification capabilities for pulmonary nodule malignancy.

3.9 Different depths of ResNet

The influence of different depths of ResNet on performance is investigated through experiments examining various architectures. As shown in Figure 6, results indicate that as the depth of ResNet increases, performance initially improves due to enhanced capabilities in capturing complex features and learning intricate hierarchical representations. This improvement arises because deeper networks can learn more abstract representations, allowing them to model complex patterns in the data effectively. However, after reaching a certain depth, this performance stabilizes, suggesting diminishing returns regarding further depth.

Table 3: Compared with state-of-the-art methods

	Accuracy (%)	Sensitivity (%)	Specificity (%)	AUC
Nibali et al. [21]	87.85	84.88	90.74	0.875
Shen et al. [22]	86.16	83.42	88.84	0.862
Zhang et al. [23]	85.92	85.12	86.72	0.859
Wang et al. [24]	85.92	91.46	80.52	0.852
Zhang et al. [25]	90.61	91.22	90.02	0.908
Huo et al. [26]	85.08	91.71	78.62	0.841
Ding et al. [27]	84.96	84.39	85.51	0.847
Manzari et al. [28]	84.72	87.56	81.95	0.853
Ours	91.34	92.44	90.26	0.924

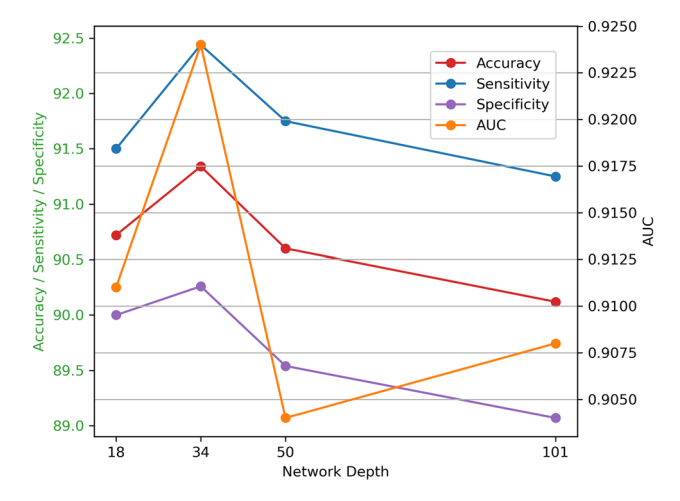


Figure 6: Comparisons with different depths.

The saturation occurs because very deep networks may struggle with issues like overfitting and increased difficulty during training. Overall, while increasing depth enhances classification performance up to a point by leveraging these advanced capabilities, careful consideration is necessary regarding training dynamics and computational resources in deeper configurations.

4 Conclusion

In this article, we present innovative strategies to enhance the effectiveness of image classification for classifying pulmonary nodule malignancy. Our approach addresses limitations in previous methods, notably the inadequate integration of multiscale features and the suboptimal use of conventional loss functions. By implementing multiscale feature weighted fusion, we improve information integration across various scales, allowing our model to focus on key pixel positions essential for accurate diagnosis. Furthermore, the combination of contrastive loss with binary cross entropy facilitates superior learning from similarities and differences among paired samples, enhancing discrimination between similar nodules while maintaining sensitivity to class variations. The results demonstrate that our methodologies yield improvements in classification performance and reliability compared to existing approaches. Looking ahead, future research could explore further optimization of feature integration techniques and investigate additional hybrid loss functions that leverage more complex relationships within datasets, aiming to refine diagnostic accuracy even further and expand applications to other medical imaging scenarios.

Funding information: This research received no external funding.

Author contributions: Ping Zhang and Li Cheng developed the conceptual framework. Li Cheng handled data collection and analysis, while Jian Mao oversaw the project and ensured result integrity. All authors contributed to drafting and revising the manuscript.

Conflict of interest: The authors declare that there is no conflict of interest regarding the publication of this article.

Ethical approval: This research was based on publicly available data and did not involve any direct interaction with human subjects or use of animal subjects. Therefore, ethical approval was not applicable.

Data availability statement: The data used to support the findings of are available on: https://www.cancerimagingarchive.net/collection/lidc-idri/.

References

- [1] A. McWilliams, M. C. Tammemagi, J. R. Mayo, H. Roberts, G. Liu, K. Soghrati, et al., "Probability of cancer in pulmonary nodules detected on first screening CT," *New Engl. J. Med.*, vol. 369, no. 10, pp. 910–919, 2013.
- [2] A. E. Prosper, M. N. Kammer, F. Maldonado, D. R. Aberle, and W. Hsu, "Expanding role of advanced image analysis in ct-detected indeterminate pulmonary nodules and early lung cancer characterization," *Radiology*, vol. 309, no. 1, p. e222904, 2023.
- [3] M. Javaid, M. Javid, M. Z. U. Rehman, and S. I. A. Shah, "A novel approach to CAD system for the detection of lung nodules in CT images," *Comput. Methods Programs Biomed.*, vol. 135, pp. 125–139, 2016.
- [4] R. Yuan, P. M. Vos, and P. L. Cooperberg, "Computer-aided detection in screening CT for pulmonary nodules," *Am. J. Roentgenol.*, vol. 186, no. 5, pp. 1280–1287, 2006.
- [5] Y. Liu, Y. Balagurunathan, T. Atwater, S. Antic, Q. Li, R. C. Walker, et al., "Radiological image traits predictive of cancer status in pulmonary nodules," *Clin. Cancer Res.*, vol. 23, no. 6, pp. 1442–1449, 2016. doi: http://dx.doi.org/10.1158/1078-0432.ccr-15-3102.
- [6] J. R. Ferreira, M. C. Oliveira, and P. M. de Azevedo-Marques, "Characterization of pulmonary nodules based on features of margin sharpness and texture," J. Digit. Imag., vol. 31, no. 4, 451–463, 2017. doi: http://dx.doi.org/10.1007/s10278-017-0029-8.
- [7] S.-J. Tu, C.-W. Wang, K.-T. Pan, Y.-C. Wu, and C.-T. Wu, "Localized thin-section ct with radiomics feature extraction and machine learning to classify early-detected pulmonary nodules from lung cancer screening," *Phys. Med. Biol.*, vol. 63, 065005, 2018, doi: http://dx.doi.org/10.1088/1361-6560/aaafab.
- [8] J. Yang, H. Wang, C. Geng, Y. Dai, and J. Ji, "Advances in intelligent diagnosis methods for pulmonary ground-glass opacity nodules," *BioMed. Eng. OnLine*, vol. 17, no. 1, 20, 2018, doi: http://dx.doi.org/ 10.1186/s12938-018-0435-2.

- [9] J. Uthoff, M. J. Stephens, J. D. Newell, E. A. Hoffman, J. Larson, N. Koehn, et al., "Machine learning approach for distinguishing malignant and benign lung nodules utilizing standardized perinodular parenchymal features from CT," *Med. Phys.*, vol. 46, no. 7, pp. 3207–3216, 2019, doi: http://dx.doi.org/10.1002/mp.13592.
- [10] A. Yamada, A. Teramoto, M. Hoshi, H. Toyama, K. Imaizumi, K. Saito, and H. Fujita, "Hybrid scheme for automated classification of pulmonary nodules using pet/CT images and patient information," *Appl. Sci.*, vol. 10, no. 2, 4225, 2020, doi: http://dx.doi.org/10.3390/ app10124225.
- [11] K. Chen, Y. Nie, S. Park, K. Zhang, Y. Zhang, Y. Liu, et al., "Development and validation of machine learning-based model for the prediction of malignancy in multiple pulmonary nodules: Analysis from multicentric cohorts," Clin. Cancer Res., vol. 27, no. 8, pp. 2255–2265, 2021, doi: http://dx.doi.org/10.1158/1078-0432.ccr-20-4007.
- [12] M. Liu, Z. Zhou, F. Liu, M. Wang, Y. Wang, M. Gao, et al., "Ct and CEA-based machine learning model for predicting malignant pulmonary nodules," *Cancer Sci.*, vol. 113, no. 12, pp. 4363–4373, 2022. doi: http://dx.doi.org/10.1111/cas.15561.
- [13] H. Wang, T. Zhao, L. C. Li, H. Pan, W. Liu, H. Gao, et al., "A hybrid CNN feature model for pulmonary nodule malignancy risk differentiation," J. X-Ray Sci. Tech., vol. 26, no. 2, pp. 171–187, 2017. doi: http://dx.doi.org/10.3233/xst-17302.
- [14] Q. Dou, H. Chen, L. Yu, J. Qin, and P.-A. Heng, "Multilevel contextual 3-D CNNs for false positive reduction in pulmonary nodule detection," *IEEE Trans. Biomed. Eng.*, vol. 64, no. 7, 2017, pp. 1558–1567, doi: http://dx.doi.org/10.1109/tbme.2016.2613502.
- [15] H. Jin, Z. Li, R. Tong, and L. Lin, "A deep 3D residual CNN for false-positive reduction in pulmonary nodule detection," *Med. Phys.*, vol. 45, no. 5, pp. 2097–2107, 2018. doi: http://dx.doi.org/10.1002/mp. 12846
- [16] X. Feng, J. Yang, A. F. Laine, and E. D. Angelini, "Discriminative localization in cnns for weakly-supervised segmentation of pulmonary nodules," *Multimodal Brain Image Anal.*, vol. 10435, pp. 568–576, 2017. doi: http://dx.doi.org/10.1007/978-3-319-66179-7_65.
- [17] X. Zhao, S. Qi, B. Zhang, H. Ma, W. Qian, Y. Yao, and J. Sun, "Deep CNN models for pulmonary nodule classification: Model modification, model integration, and transfer learning," *J. X-Ray Sci. Tech.*, vol. 27, no. 4, pp. 615–629, 2019, doi: http://dx.doi.org/10. 3233/xst-180490.
- [18] B.-C. Kim, J. S. Yoon, J.-S. Choi, and H.-I. Suk, "Multi-scale gradual integration cnn for false positive reduction in pulmonary nodule

- detection," *Neural Netw.*, vol. 115, no., pp. 1–10, 2019, doi: http://dx.doi.org/10.1016/j.neunet.2019.03.003.
- [19] Y. Xu, S. Wang, X. Sun, Y. Yang, J. Fan, W. Jin, et al., "Identification of benign and malignant lung nodules in CT images based on ensemble learning method," *Interdiscipl. Sci. Comput. Life Sci.*, vol. 14, no. 1, pp. 130–140, 2022, doi: http://dx.doi.org/10.1007/s12539-021-00472-1.
- [20] H. Yuan, Z. Fan, Y. Wu, and J. Cheng, "An efficient multi-path 3D convolutional neural network for false-positive reduction of pulmonary nodule detection," *Int. J. Comput. Assisted Radiol. Surgery*, vol. 16, pp. 2269–2277, 2021, doi: http://dx.doi.org/10.1007/s11548-021-02478-y.
- [21] A. Nibali, Z. He, and D. Wollersheim, "Pulmonary nodule classification with deep residual networks," *Int. J. Comput. Assist. Radiol. Surgery*, vol. 12, pp. 1799–1808, 2017.
- [22] W. Shen, M. Zhou, F. Yang, C. Yang, and J. Tian, "Multi-scale convolutional neural networks for lung nodule classification," in Information Processing in Medical Imaging: 24th International Conference, IPMI 2015, Sabhal Mor Ostaig, Isle of Skye, UK, June 28–July 3, 2015, Proceedings 24. Springer, 2015, pp. 588–599.
- [23] G. Zhang, D. Zhu, X. Liu, M. Chen, L. Itti, Y. Luo, and J. Lu, "Multi-scale pulmonary nodule classification with deep feature fusion via residual network,", J. Ambient Intel. Humanized Comput., vol. 14, pp. 1–12, 2023.
- [24] Y. Wang, H. Zhang, K. J. Chae, Y. Choi, G. Y. Jin, and S.-B. Ko, "Novel convolutional neural network architecture for improved pulmonary nodule classification on computed tomography," *Multidimen. Syst. Signal Proces.*, vol. 31, pp. 1163–1183, 2020.
- [25] Y. Zhang, J. Zhang, L. Zhao, X. Wei, and Q. Zhang, "Classification of benign and malignant pulmonary nodules based on deep learning," in 2018 5th International Conference on Information Science and Control Engineering (ICISCE). IEEE, 2018, pp. 156–160.
- [26] X. Huo, G. Sun, S. Tian, Y. Wang, L. Yu, J. Long, et al., "Hifuse: Hierarchical multiscale feature fusion network for medical image classification," *Biomed. Signal Proces. Control*, vol. 87, p. 105534, 2024.
- [27] Z. Ding, H. Li, Y. Guo, D. Zhou, Y. Liu, and S. Xie, "M4fnet: Multimodal medical image fusion network via multi-receptive-field and multiscale feature integration," *Comput. Biol. Med.*, vol. 159, p. 106923, 2023.
- [28] O. N. Manzari, H. Ahmadabadi, H. Kashiani, S. B. Shokouhi, and A. Ayatollahi, "Medvit: a robust vision transformer for generalized medical image classification," *Comput. Biol. Med.*, vol. 157, p. 106791, 2023.